AIAA JOURNAL
Vol. 34, No. 3, March 1996

Study of Aircraft Wake Vortex Behavior Near the Ground

Z. C. Zheng* and Robert L. Ash†
Old Dominion University, Norfolk, Virginia 23529-0247

Aircraft wake vortices have been modeled using an unsteady, two-dimensional laminar (constant eddy viscosity) approximation of the Navier–Stokes equations, to study the influence of ground coupling, stratification, and crosswind on vortex system behavior and decay. Initialization and boundary conditions are developed and implemented systematically for a nonuniform grid representation of the semi-infinite domain containing a vortex pair. Subsequently, the physics of wake vortex interactions with the ground for different types of surface weather conditions are discussed.

Nomenclature

a, b = constants
B_n = Fourier coefficient
C_L = lift coefficient
C_l = rolling moment coefficient
c = chord length
c_p = specific heat at constant pressure
g = acceleration of gravity
L = aircraft weight (lift)
N, N^* = Brunt–Väisälä frequency
p = pressure
r = radius
s_0 = half-span
T_∞, T_0 = ambient temperature, reference temperature
t = time
$\bar{t}$ = $\Gamma_0 t/s_0^2$
U_F = flight speed of follower aircraft
U_∞ = flight speed or characteristic crosswind velocity
u, v = local horizontal and vertical velocity components
x, y = Cartesian coordinates
α = angle of attack
β = thermal lapse rate
Γ_0 = initial circulation
γ = ratio of specific heats
δ = crosswind boundary-layer thickness
ζ = vorticity
η = inner similarity variable
ν = kinematic viscosity
$\rho, \tilde{\rho}$ = density
Φ = Oseen function
ψ = stream function

I. Introduction

THE avoidance of wake vortex encounters by following aircraft during landing and takeoff is considered to be the primary requirement controlling aircraft spacing around congested airports.[1] The powerful axial wake vortex pair produces rotational forces that can override the control authority of many aircraft. Those vortices have circulation levels that scale directly with the size and speed of the generating aircraft and persist as tightly wound rotating flows for significant distances. This type of hazard is a major concern because aircraft in terminal flight can maintain only limited separations while following converging flight paths—very near the ground. Descending wake vortex pairs maintain almost rigid spacing during cruising flight, but interactions with the ground during terminal flight alter their trajectories, causing them to spread.

Received Dec. 24, 1994; revision received Oct. 5, 1995; accepted for publication Oct. 17, 1995.

*Research Assistant Professor, Aerospace Engineering Department. Member AIAA.
†Professor, Aerospace Engineering Department. Associate Fellow AIAA.

Potential flow theory predicts hyperbolic trajectories during a wall encounter, and the separate vortices asymptote toward their initial half-spacing height as they spread apart.[2] However, aircraft wake vortices generate viscous boundary-layer flows (opposite sign vorticity) along the ground that can separate and cause the primary vortices to rebound vertically, thus departing from their hyperbolic paths. The simultaneous effects of ground boundary-layer coupling and crosswind can cause these rebounding wake vortices to migrate either into the operational flight path of a parallel runway or to remain and even rise into the original flight path along a single runway. Potential flow theory can neither predict that type of wake vortex motion near the ground nor quantify the rate of decay. We have been engaged in numerical studies directed toward modeling the behavior of aircraft wake vortices near the ground, in support of a much larger overall research program at NASA Langley Research Center.[3]

Because of the importance of vorticity theory in aerodynamics, a considerable body of literature exists concerning aircraft trailing line vortex systems (see Donaldson and Bilanin[4] for an excellent summary of the work up to 1975). Unfortunately, that literature relies heavily on inviscid theory, restricting its utility in predicting any kind of atmospheric or ground coupling and precluding the inclusion of viscous decay. The vortex rollup process, immediately behind the aircraft, is also problematic but is assumed to be complete in this study.

Dee and Nicholas[5] first reported vortex rebound in an experimental study of smoke-marked aircraft vortices near the ground. The rebound phenomenon could not be explained via inviscid theory.[6] Harvey and Perry[7] conjectured that rebound behavior resulted from separation of the vortex-induced surface boundary layer, during vortex–ground encounter. Other explanations have been proposed,[8] but ground-layer flow separation has been demonstrated in virtually all realistic vortex–surface encounter conditions, except at very low Reynolds numbers.[9] Aircraft wake vortices are high Reynolds number flows, and the goal of our numerical studies is to predict reliably the paths followed by the two fully evolved vortices, within a realistic environmental region, while simultaneously predicting their rates of decay. Only then can the numerical model be used to help forecast vortex hazard conditions around airports.

Several theoretical and numerical models have been employed previously to study vortex–wall encounters. Walker,[10] Ersoy and Walker,[11] and Doligalsky et al.[12] have exploited the connection between wake vortices and turbulent boundary-layer flow structures in their boundary-layer-theory-based studies of vortex–wall encounters. That approach provides an excellent method for estimating both the time and the location of the onset of separation along the surface, but unfortunately the boundary-layer restrictions are violated as soon as flow separation is initiated. Since we are concerned with the subsequent behavior of the vortex systems during and after separation, numerical techniques were required that avoided the boundary-layer restrictions. Although finite difference solutions of the Navier–Stokes equations cannot capture flow separation as accurately as the boundary-layer models, the fully elliptic numerical approaches are able to proceed past the onset of separation. Peace and

Riley[9] have used a Navier–Stokes based approach, as has Orlandi.[13] Peace and Riley's approach,[9] however, was unable to match the inner and outer pressure fields during their flow initialization and Orlandi[13] used a computational domain whose dimensions did not approximate the semi-infinite half-space representing the aircraft wake vortex problem.

The influences of atmospheric effects on vortex decay have been studied by Bilanin et al.[14,15] and Teske et al.[16] Greene[17] has developed an approximate model for predicting the influence of atmospheric effects on wake motion and decay away from the ground. Only limited experimental observations have been reported that are concerned with actual aircraft wake vortex encounters with the ground,[5,18,19] whereas laboratory studies have been reported that have measured vortex trajectories under more controlled conditions than can be managed in the field. Liu and Srnsky[20] and Delisi et al.[21] have used airfoil devices in tow-tank or tilt-tank facilities, whereas Barker and Crow[8] used a submerged apparatus that shed a pair of axial vortices in a tank. All of these laboratory studies were necessarily conducted at Reynolds numbers that were much lower than those associated with aircraft flight.

At flight Reynolds numbers, turbulent vortex cores are very small in comparison with the wing span of the generating aircraft. Even during terminal flight, the vortex core regions remain small for very long distances and times,[18] finally dissipating after strong interactions with the ground. Current turbulence models[15,22,23] cannot simulate the observed small core behavior and, therefore, cannot predict vortex trajectories and decay reliably. Previously, turbulence effects have been accommodated crudely by using simple eddy viscosity corrections.[24] More recently, Zeman[25] has determined that the global behavior of prototype aircraft wake vortex systems is controlled more by viscosity than by turbulence. Hence, it is possible in principle to adjust viscosity to account for full-scale effects, modeling overall viscous decay with an essentially laminar model that smears out the vortex core details over larger physical volumes. This associated core dilation produces inaccuracies in predicting trajectories, but can model overall decay.

Simulation of the wake vortex–ground encounter problem presents a variety of numerical challenges. Besides the difficulties associated with viscous surface layer regions, the need to properly model vortex cores requires a relatively fine numerical grid well away from the surface region. Since the combined multiple vortex–wall problem cannot be initialized via any type of exact solution, the numerical startup transients that are inherent in transforming inviscid representations of vortices near a solid boundary to viscous simulations must also be controlled. Both Reynolds number limits and turbulence models must be addressed. Finally, modeling an elliptic system over a semi-infinite domain requires either a grid stretching technique or construction of alternative boundary conditions at locations other than their infinite limits.

The current numerical study has concentrated on simulating unsteady vortex motion in proximity with the ground over time intervals that are representative of terminal flight operations. Hence, we have considered 1) the merging of vortex core and ground plane viscous zones, 2) the formation and evolution of secondary and tertiary vortices via coupling with the ground, and 3) long-term trajectory predictions, including decay and interpretation of hazard potential. We have utilized a vorticity-stream function formulation with discretization over a stretched, nonuniform grid spanning the semi-infinite half-space. We have used consistent boundary conditions for the infinite limits, thereby representing the far-field boundary conditions properly. The flow was initialized using a two-parameter matched asymptotic expansion technique[26] that permitted velocity and pressure matching between the inner and outer flow regimes, eliminating detectable oscillations during initiation of the time marching scheme. Although upwind flux-splitting was tested for the convection terms, the Arakawa[27] scheme was selected because it exhibited superior grid independence at high Reynolds numbers.

II. Numerical Model

The aircraft wake vortex system has been modeled initially as a two-dimensional vortex pair in a viscous fluid. A particular aircraft

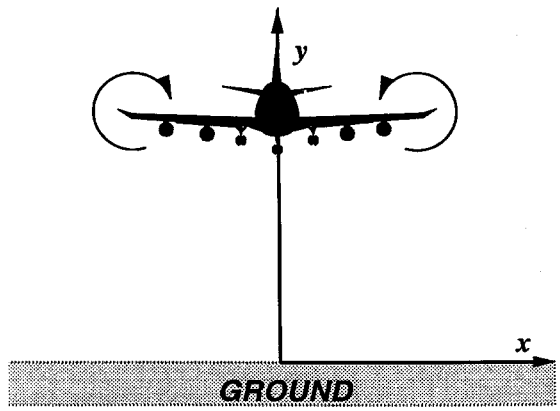

Fig. 1 Schematic of wake vortex representation and associated coordinate system.

is represented as a pair of vortices whose circulations $\pm\Gamma_0$ are given by

$$\Gamma_0 = \frac{L}{2\rho s_0 U_\infty} \tag{1}$$

We have neglected the initial vortex rollup phase, and the vortex pair was started at a specific height. The initial system is depicted schematically in Fig. 1. The initial (specified) vortex locations had to be close enough to the ground plane to avoid wasting computational resources, but also had to be far enough from the ground to permit the evolution of the viscous vortex cores and their associated unsteady viscous boundary layers (along the ground), prior to strong interactions with the ground plane.

Aircraft wake vortices are turbulent, high Reynolds number, three-dimensional flows and cannot be resolved fully with any existing computational resources. This study is concentrated on laminar-like simulation, for the reasons already stated. To use a two-dimensional model, it is important to identify some of the flow features that are neglected a priori. Specifically, the initial wake vortices include high-velocity axial jets (in the direction opposite to the line of flight),[28] and these axial jets that imply minimum pressure regions along the vortex axes probably burst immediately behind the aircraft, becoming low-speed axial wakes. There are rigorous theoretical links between the expansion of the vortex core regions and local axial pressure gradients,[29,30] and those constraints are excluded automatically by a two-dimensional model. Also, during strong ground coupling, it is possible that vortex bending and stretching can produce important flow effects that will not be captured by the two-dimensional model. When compared to any type of inviscid approximation, however, the inclusion of ground coupling and the ability to estimate decay rates are important features that can be gained within the current two-dimensional approximations.

We have discussed the justification for using Boussinesq approximations to model stratified atmospheric environments near the ground earlier.[23,31] In atmospheric flows, where both ambient pressure and temperature vary with elevation, it is conventional to employ potential temperature, $T_p(y) \equiv T_\infty(y)[p(y)/p(0)]^{(\gamma-1)/\gamma}$ that allows for departures from an adiabatic lapse rate in interpreting local temperature (see Landau and Lifshitz[32]). In the present study, however, the small elevation interval over which ground coupling was considered produces negligible effects of atmospheric pressure change. Hence, we have employed ambient temperature, where

$$T_\infty(y) = T_0 + \beta y \tag{2}$$

represents the first term in a polynomial fit. If the corresponding ambient density profile is represented as $\rho_\infty(y)$, then the normalized density departure $\tilde{\rho}$ can be defined by

$$\tilde{\rho} = \frac{\rho(x, y, t) - \rho_\infty(y)}{\rho_0} \tag{3}$$

where $\rho_0 = \rho_\infty(0)$ is the characteristic undisturbed density. The evolution of $\tilde{\rho}$ is governed by

$$\frac{\partial \tilde{\rho}}{\partial t} + \frac{\partial(\tilde{\rho}u)}{\partial x} + \frac{\partial(\tilde{\rho}v)}{\partial y} = -\frac{v}{\rho_0}\frac{d\rho_\infty}{dy} \tag{4}$$

This equation can be derived as either a complementary conservation of mass requirement or from conservation of energy considerations. Either way, the two-dimensional, unsteady velocity field must satisfy the continuity requirement

$$\frac{\partial u}{\partial x} + \frac{\partial v}{\partial y} = 0 \tag{5}$$

A vorticity-stream function computational model was developed and implemented by Zheng[31] to simulate wake vortex behavior via the vorticity transport equation,

$$\frac{\partial \zeta}{\partial t} + \frac{\partial(u\zeta)}{\partial x} + \frac{\partial(v\zeta)}{\partial y} = \nu\nabla^2\zeta - g\frac{\partial \tilde{\rho}}{\partial x} \tag{6}$$

and the corresponding (Poisson) stream function equation,

$$\nabla^2\psi = -\zeta \tag{7}$$

Here, vorticity ζ and stream function ψ are defined by

$$\zeta = \frac{\partial v}{\partial x} - \frac{\partial u}{\partial y}, \qquad u = \frac{\partial \psi}{\partial y}, \qquad \text{and} \qquad v = -\frac{\partial \psi}{\partial x} \tag{8}$$

Unstratified vortex behavior ($\partial\rho_\infty/\partial y = 0$) is simulated by setting $\tilde{\rho} = 0 = \text{const}$.

In the absence of crosswinds, the vortex pair interacts symmetrically with the ground, and the simulations can be accomplished in the first quadrant via symmetry conditions along $x = 0$. In those cases, a 150×300 numerical grid was employed using nonuniform spacing. The spacing between grid points was effected via an exponential mapping that transformed the $0 \le x < \infty, 0 \le y < \infty$ domain into a finite rectangular region. Not only could the far-field boundary conditions be made to approximate the actual infinite domain requirements (discussed subsequently), but the grid points along the vortex core trajectories and along the ground plane could be packed to resolve the regions with significant (viscous) gradients. When crosswinds were considered, the numerical grid was reflected across the $x = 0$ plane, producing a 300×300 network. In addition, that grid was convected with a constant (cross wind) velocity, to retain high resolution of the viscous core zones.

Near the ground, the unsteady viscous layers must evolve properly along the surface; under some conditions they must evolve into time-varying separation zones (opposite sign vorticity) and react with the primary wake vortices to cause rebound. As already mentioned, the vortex pair must be started far enough from the ground plane to permit the viscous wall regions to evolve properly without using excessive computational resources. We have found that an initial height equal to the nominal wing span of the generating aircraft ($y_0 = 2s_0$) is a good compromise between resolution and computational resource requirements.

Depending on whether symmetry or inflow/outflow boundary conditions are employed, the size of the computational domain is altered between crosswind and no crosswind (symmetric) simulations. The appropriate vorticity and stream function boundary conditions for the two cases are

$$\frac{\partial \psi}{\partial y}(\pm\infty, y, t) = U_\infty(y) \quad \text{or} \quad \psi(0, y, t) = \psi(\infty, y, t) = 0 \tag{9}$$

for the crosswind domain and the symmetry plane domain, respectively, and

$$\zeta(\pm\infty, y, t) = -\frac{dU_\infty}{dy}(y) \quad \text{or} \quad \zeta(0, y, t) = \zeta(\infty, y, t) = 0 \tag{10}$$

$$\psi(x, \infty, t) = 0 \tag{11}$$

and

$$\zeta(x, \infty, t) = 0 \tag{12}$$

Along the ground plane boundary, we require that

$$\psi(x, 0, t) = 0 \tag{13}$$

and

$$\zeta(x, 0, t) = -\frac{\partial^2 \psi}{\partial y^2}(x, 0, t) \tag{14}$$

Zheng[31] has developed a matched asymptotic expansion technique to initialize the vortex flow system, prior to the finite difference-based numerical simulations. In that approach, velocity and pressure matching have been imposed between inner and outer expansions representing the initial, nonsimilar viscous boundary layers along the rigid surface. Thus, the numerical simulation can avoid the nonphysical discontinuities that would be imposed by placing a pair of point vortices in a viscous fluid outside of the boundary-layer zones. The vortex pair was treated as two isolated Oseen vortices (and their images) located at $(\pm s_0, 2s_0)$ during initiation of the numerical simulations. (It should be noted that the vortex pair has an initial separation given by $2\pi s_0/4$, but at $y_0 = 2s_0$, the vortex pair has already begun to separate. If potential flow theory can be applied, s_0 should be 88% of the actual aircraft half-span.) Furthermore, at the time of initialization, the Oseen vortex core radii r_c were assumed to have expanded to $0.2s_0$, defined in terms of the location of maximum swirl velocity. The initial flowfield was approximated (outside of the boundary-layer regions) by the velocity distributions

$$u(x, y, 0) = (y - 2s_0)[\Phi(x, y; s_0, 2s_0) - \Phi(x, y; -s_0, 2s_0)] + (y + 2s_0)[\Phi(x, y; s_0, -2s_0) - \Phi(x, y; -s_0, -2s_0)] \tag{15}$$

and

$$v(x, y, 0) = (x - s_0)[\Phi(x, y; s_0, 2s_0) - \Phi(x, y; s_0, -2s_0)] + (x + s_0)[\Phi(x, y; -s_0, -2s_0) - \Phi(x, y; -s_0, 2s_0)] \tag{16}$$

where

$$\Phi(x, y; a, b) = \frac{\Gamma_0}{2s_0\pi}\frac{1 - \exp\left\{-[(x-a)^2 + (y-b)^2]/r_c\right\}}{(x-a)^2 + (y-b)^2} \tag{17}$$

The asymptotic expansions produced analytic solution representations for the stream function within the unsteady laminar boundary-layer region. In that zone, the initialization stream function was given by

$$\psi(x, y, 0) = 2\Gamma_0\left[(\sqrt{\nu t_0}/s_0)\psi_1(x, \eta, t_0) + \left(\nu t_0/s_0^2\right)\psi_2(x, \eta, t_0) + \cdots\right] \tag{18}$$

Here, t_0 is the truncation time used to terminate the asymptotic representation and for subsequently initiating the finite difference simulations; typically, t_0 was taken to be $0.1s_0^2/\Gamma_0$. The similarity variable is defined by $\eta = y/\sqrt{(4\nu t_0)}$. Unfortunately, ψ_1 and ψ_2 are rather complicated and have been tabulated elsewhere.[26,31]

The far-field boundary conditions cannot be applied at infinity. When the 150×300 grid was used, the associated coordinate mappings produced final finite x and y locations at $25s_0$ and $11.4s_0$, respectively. No difficulties were encountered via the mapping procedure.

Conversely, Gresho[33] has discussed the difficulties associated with applying vorticity boundary conditions along a wall. It was necessary to represent the vorticity boundary condition [Eq. (14)] at the first vertical grid location to avoid inconsistencies. The resulting boundary condition appears formally to be second-order accurate, but is in fact only first-order accurate because of its associated wall velocity boundary condition.[34] However, the very fine, nonuniform grid spacing along the wall was exploited properly via our consistent first-order vorticity boundary condition.

First-order, time-accurate schemes were used for numerical integration of the vorticity transport equation and the density departure equation. Central differencing was used for the diffusion terms in the vorticity transport equation. Arakawa's[27] explicit second-order scheme was employed for the advective terms after it was found to exhibit superior grid independence when compared with results using an alternating direction implicit scheme with flux splitting for the convective terms. The stream function equation is a standard Poisson form and was integrated using the Poisson solver developed by Swartztrauber and Sweet.[35] The iteration residual, based on output from that solver, showed that it could achieve integration accuracies equivalent to the order of 10^{-8}. The accuracy of the stream function calculations was found to be a critical concern in predicting vortex rebound behavior reliably.

Grid sensitivity was tested for a symmetric flow (to minimize computational resource requirements) at circulation-based Reynolds numbers of 1000, 7650, and 75,000, by comparing calculations from our basic 150 × 300 grid with those obtained using a 300 × 600 grid. It was then possible to use Richardson interpolation[36] to approximate the results for even finer grids, and the 150 × 300 grid exhibited convergent results via that procedure. Grid independence was established by using the maximum vorticity within the primary vortex, both to locate the instantaneous primary vortex center and to determine the influence of the grid on numerical diffusion. For the $Re = 1000$ case, differences between instantaneous vortex center locations were less than 1%, and the maximum vorticity levels differed by less than 5%. At the upper $Re = 75{,}000$ limit, positional differences of 10% were observed, and the maximum vorticity levels differed by as much as 20%. The trajectory and magnitude sensitivities for the experimental comparison case ($Re = 7650$), were 5 and 10%, respectively.

III. Results and Discussion

We have used experimental data reported by Liu and Srnsky[20] as an additional check for our numerical simulation procedures. They measured the laminar wake vortex trajectory histories produced in an unstratified water tank by a towed NACA 0012 airfoil with a negative angle of attack. The most comprehensive data set corresponded to a vortex Reynolds number (Γ_0/ν) of 7650, and a comparison between simulated and measured trajectories, along with the horizontal position history, is shown in Fig. 2. The initial height used for this simulation was $y_0 = 3.8s_0$, in agreement with the experimental conditions. It can be seen that the simulation and measurements are in very good agreement up to a dimensionless time ($\Gamma_0 t/s_0^2$) of 100. The disagreement at later times can be attributed to a combination of experimental difficulties and inconsistencies between the numerical model and the experiment that include 1) the upper surface of the towing tank (which represented the ground plane in the experiment) consisted of two rigid floating panels on either side of an open water gap, to facilitate towing of the airfoil, thus altering the rigid surface boundary condition; 2) the water tank was of finite cross section, thus its sidewall boundaries altered the long-term vortex behavior; 3) vortex looping caused by interactions between the aging primary vortices and newly generated secondary vortices are very difficult to isolate experimentally; and 4) the actual flow boundary conditions could not be modeled numerically. It should be noted that Orlandi[13] has predicted vortex looping behavior at Reynolds numbers that approximate the Liu and Srnsky[20] data, in agreement with our simulations, but Orlandi has predicted the occurrence of multiple vortex loops during similar time intervals, which is probably because of his somewhat limited geometrical region. Orlandi's results[13] suggest that the finite extent of the towing tank should produce more vortex loops (for a true rigid surface boundary) rather than no loops. This also illuminates the difficulties associated with simulating aircraft wake vortex behavior over time intervals that are important to flight operations since the far-field boundary conditions appear to influence trajectory behavior over the interval of interest.

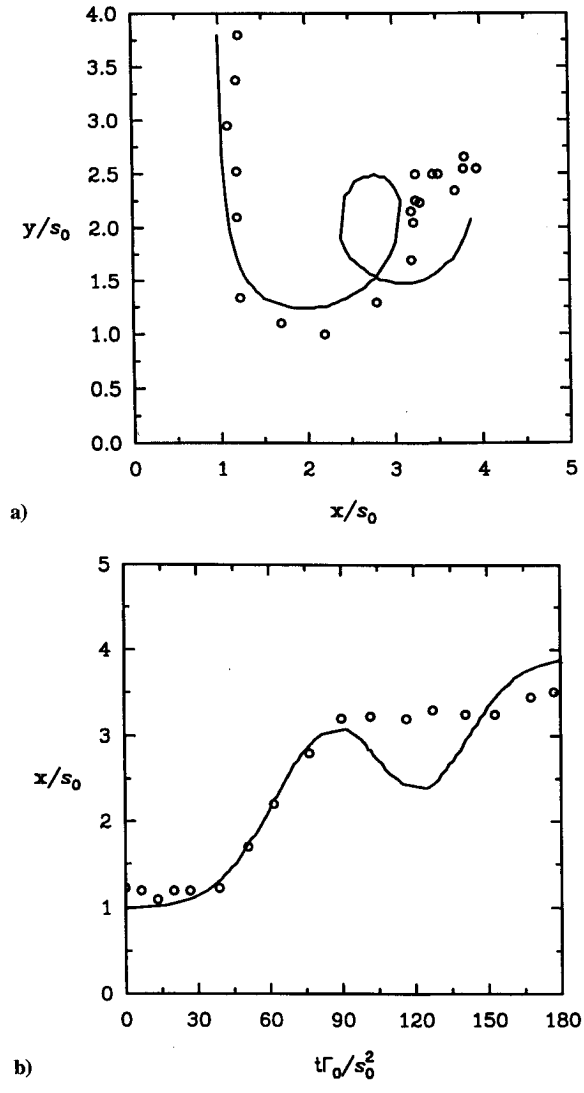

Fig. 2 Comparison at Reynolds number, Γ_0/ν = 7650 of measured and computed a) vortex trajectories and b) horizontal position histories for a vortex–wall encounter: ——, computation and o, experiment.

Reynolds Number Effects

The computed influence of vortex Reynolds number on trajectory histories is shown in Fig. 3. The x, y locations of the vortex centers are marked at time intervals of $30s_0^2/\Gamma_0$ (circles for $Re = 1000$ and plus signs for $Re = 75{,}000$), and an inviscid reference trajectory is included for comparison. It can be seen that the higher Reynolds number vortices follow trajectories that are initially very close to the inviscid model, approaching nearer to the ground than the moderate Reynolds number case. When rebound commences at the higher Reynolds number, however, the vortices move more rapidly away from the wall, reaching heights ultimately that are more than double those of their moderate Reynolds number counterparts. At the higher Reynolds numbers, the slower decay rates of both primary and secondary vortices produce stronger and more sustained coupling with the ground, resulting in multiple rebounds.

Assessment of wake vortex decay rate has been problematic since it is important to define decay as it related to hazard levels. We have examined local circulation and enstrophy (vorticity squared) histories, but neither criteria produced unambiguous trends.[26] We have thus determined that the most useful measure of decay is to use estimated maximum induced rolling moment histories.[37] That is, the instantaneous simulated velocity field can be used to produce upwash velocities $v(x_i, y_j, t_n)$ that can be used to calculate the instantaneous induced rolling moment on a representative follower aircraft wing. If the half-span of the follower wing is s_F, with an associated spanwise chord distribution given by $c(\theta)$, where

$$\theta \equiv \cos^{-1}\left[\frac{(x - x_{c_L})}{s_F}\right] \tag{19}$$

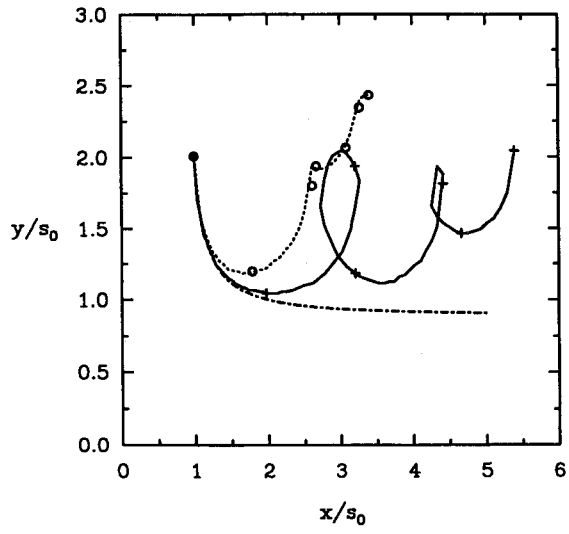

Fig. 3 Influence of Reynolds number on vortex rebound trajectories; positions are marked at $\Delta t = 30s_0^2/\Gamma_0$ intervals: ·····, potential; · · · ·, Re = 1000; and ——, Re = 75,000.

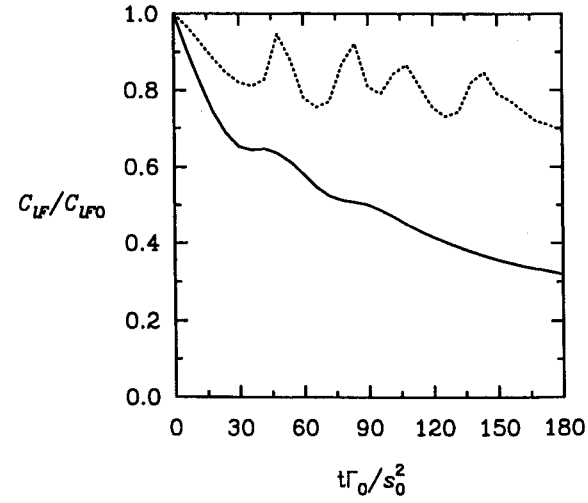

Fig. 4 Influence of Reynolds number on the decay of the maximum rolling moment coefficient: · · · ·, Re = 75,000 and ——, Re = 1000.

and x_{c_L} locates the wing midspan in the computational domain, the induced rolling moment coefficient C_l is given by

$$C_l = (\pi/16)(\partial C_L/\partial\alpha)B_2 \tag{20}$$

The coefficient B_2 is obtained from the Fourier series representation of $v(\theta)$, the computed instantaneous vertical (downwash) velocity at some elevation y, on the interval $(x_{c_L} - s_F) \leq x(x_{c_L} + s_F)$, given by

$$v(\theta) = U_F \sum_{n=1}^{\infty} B_n \frac{\bar{c}}{c(\theta)} \sin(n\theta) \tag{21}$$

where $\bar{c}$ designates the average chord and $c(\theta)$ the local chord, whereas U_F is the hypothetical speed of the following wing (assumed thus far to match the generator speed). The maximum rolling moment coefficient occurs when the follower wing center is located nominally at a vortex center. The development of this approach has been discussed in more detail by Ash et al.[37]

To quantify wake vortex decay, it was necessary to choose a representative follower wing. Our rolling moment calculations have shown that although the predicted peak rolling moment coefficients are higher initially for follower wings with spans that are smaller than the generator, the corresponding peak rolling moments decay more quickly than for large follower. When the maximum rolling moment has decayed to 63.2% of its original level, the maximum rolling moments predicted for follower wings with spans that are comparable to the generator are actually higher (in terms of their original levels) than for the smaller wings.[37] The larger follower wing, in effect, integrates the vortex core size influences out of the rolling moment coefficient distributions, thus de-emphasizing the sensitivity of the vortex hazard estimates to low Reynolds number and vortex core size effects. Therefore, the follower wing was taken to be the same span as the generator in our numerical studies. The influence of generator Reynolds number on the maximum rolling moment coefficient histories is shown in Fig. 4.

Reynolds number influences both vortex trajectories (Fig. 3) and maximum rolling moment decay history (Fig. 4). Whereas the vortices continue along their nominal inviscid paths longer at higher Reynolds numbers, their postrebound behavior is more complex, tending toward multiple bounces. The maximum rolling moment history shows complex and more gradual decay at Re = 75,000. Indeed, the maximum rolling moment history appears to be poorly resolved at Re = 75,000. However, the peculiar trajectory and uneven decay rates can be explained as follows.

From Fig. 3, it is apparent that the vortex trajectories change radically between dimensionless times ($\bar{t} = t\Gamma_0/s_0^2$) of 60 and 150, at Re = 75,000. Furthermore, an undulation in the peak rolling moment history can be observed within that time interval (Fig. 4). Those effects can be interpreted if we examine the vorticity contour plots at $\bar{t}$ = 60, 120, and 150, as shown in Fig. 5. There we see that at $\bar{t}$ = 60, the vorticity contours indicate that a secondary vortex has been shed from the wall region, while a new secondary vortex is beginning to form. Even though the secondary vortices are weaker than the primary vortex, they influence its motion (as they revolve around the primary vortex). At $\bar{t}$ = 60, the opposite sign vorticity acts to lift the primary vortex; the secondary vortex, which has been pinched off from the wall, acts to retard the lateral motion of the primary vortex. At $\bar{t}$ = 120, the secondary vortex resides directly above the primary vortex and can strongly retard its lateral motion. At the same time, however, a new secondary vortex of comparable strength to the shed vortex is forming. As time proceeds to $\bar{t}$ = 150, the new secondary vortex becomes stronger than the original shed vortex, but the older vortex has revolved into closer proximity to the left side of the primary vortex. For a brief time interval (near $\bar{t}$ = 150), the two secondary vortices tend to compensate, allowing the primary vortex to revert toward its original, nearly inviscid, vortex-pair wall interaction (but with greater separations and weaker strengths). This process can continue, but with ever increasing numbers of weakening, shed vortices.

The complexity of the rolling moment history can be explained similarly using Fig. 5. At $\bar{t}$ = 60, the secondary vortex is positioned to augment the vertical velocity on the outboard side of the primary vortex. Hence, during some time interval, the contribution from the secondary vortex can increase the instantaneous rolling moment and offset the decay of the primary vortex. As the secondary vortex rotates above the primary vortex ($\bar{t}$ = 120), it ceases to augment the maximum rolling moment, along the line connecting the primary vortices. Finally, at $\bar{t}$ = 150, the pair of secondary vortices can both make small local contributions to the rolling moment as the maximum rolling moment reverts toward its unmodified primary vortex behavior.

At Re = 1000, these compound effects are nearly undetectable because of viscous diffusion and dissipation. At the lower Reynolds numbers, the shed vortices dissipate rapidly and exert only minor influences on the primary vortex. Hence, at low Reynolds numbers, the primary vortices are strongly coupled with the viscous zone along the ground plane, whereas the shed vortices are widely diffused and too weak to alter the primary motion. Of course, the same mechanisms that dissipate the shed vortices also act to dissipate the primary vortices more rapidly.

Buoyancy

Atmospheric stratification is typically the only mechanism that can reverse the downward motion of an aircraft wake away from the ground. When the atmosphere is stably stratified, the ambient temperature increases with height. Under stably stratified conditions, the velocity field, set up by a descending wake vortex pair, induces a flow of warmer fluid from above the vortex pair into their core regions. As a result, buoyant forces act on the vortex pair,

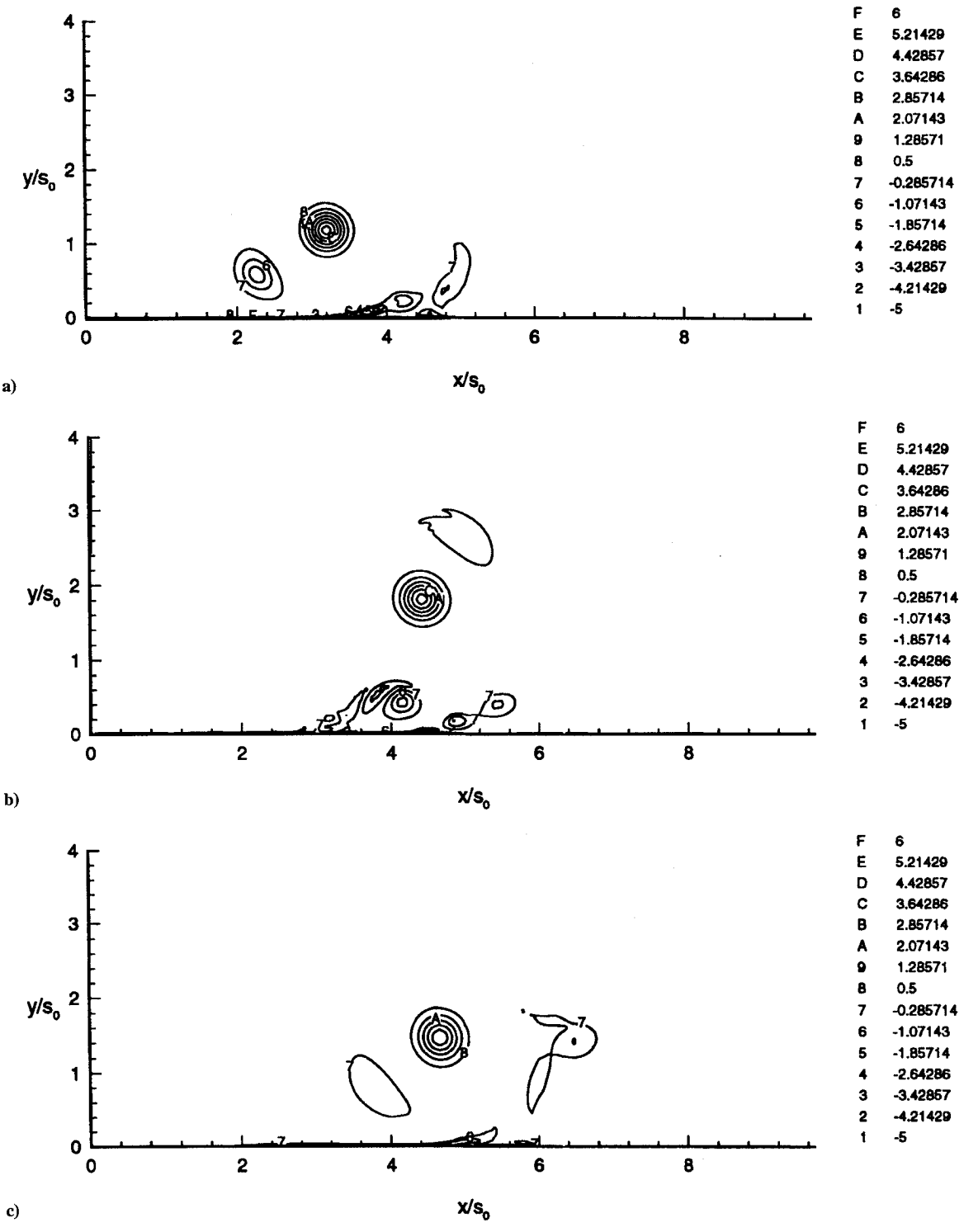

Fig. 5 Vorticity contour plots for a symmetric, unstratified vortex–wall encounter at $Re = 75{,}000$, $\bar{t} = \Gamma_0 t/s_0^2 =$: a) 60, b) 120, and c) 150.

reversing their descent. Buoyant forces are parameterized in terms of the Brunt–Väisälä frequency N^*, where

$$(N^*)^2 = -\frac{g}{\rho_0}\frac{\mathrm{d}\rho_\infty}{\mathrm{d}y} = \frac{g}{T_0}\left[\beta + \frac{g}{c_p}\right] \tag{22}$$

where β and T_0 are given in Eq. (2). Brunt–Väisälä frequencies as high as 0.02 1/s are common near the ground, and correspond to a dimensionless frequency $N = N^* s_0^2/\Gamma_0$ of approximately 0.01 for flight conditions.

Equations (4) and (6) show how buoyant forces act to alter the vorticity distribution and thus affect vortex structures. From the right-hand side of Eq. (4), we see that the density departure, following a particle, is related directly to the vertical motion of fluid particles (in the stratified fluid). Thus, the horizontal gradient in density departure, appearing in Eq. (6), can be related directly to gradients in vertical position change following particles. That is, if two particles separated by a small distance $\mathrm{d}x$ were located at the same elevation, say, y_0, at some time t in the stratified fluid, the particle that has been subjected to the largest overall vertical displacement produces a larger density departure (either by heavier fluid moving upward or by lighter fluid moving downward). Furthermore, if the particle on the right $(x + \mathrm{d}x)$ has moved farther upward than the particle on its left, in arriving at y_0 (at time t), a clockwise torque is produced by the heavier outboard fluid. Conversely, for greater downward outboard motion, a larger penetration displacement on

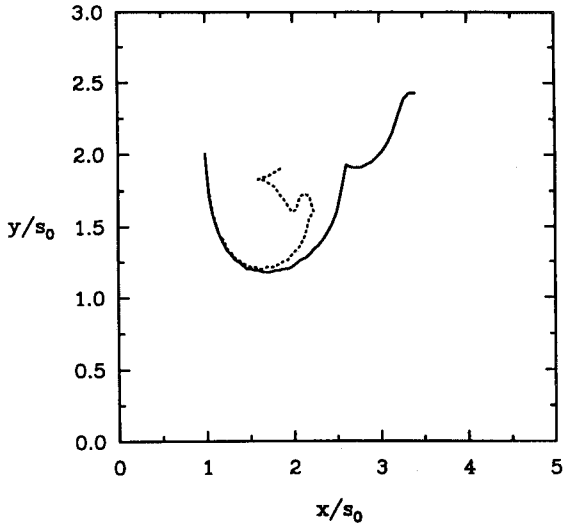

Fig. 6 Influence of stratification on vortex trajectories: Re = 1000, no crosswind: ——, N = 0 and - - - -, N = 0.04.

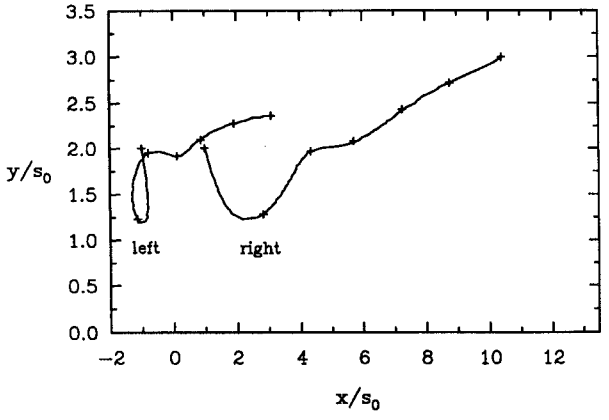

Fig. 7 Influence of crosswind on asymmetric vortex trajectories; Re = 1000, $\delta = 10s_0$, and $U_\infty = 0.1\Gamma_0/s$.

the right creates a counterclockwise torque via buoyancy acting on the lighter outboard fluid.

Along the ground plane, buoyancy effects cannot occur, since there is no vertical motion. Away from the boundary, however, viscous and buoyant forces are both operative. It can be seen that vorticity will be produced around inviscid structures via Eq. (6), and viscosity will moderate those effects. Therefore, as a wake vortex pair moves through a stratified atmosphere, it will depart from its potential vortex pair configuration, acted on ultimately by viscous forces. It is also obvious that there will be limits to the extent of vertical motion (both up and down) through which a fluid particle can move, since the buoyant forces will increase continuously until particles finally reverse direction. Therefore, the influence of stratification will always affect vortex behavior, becoming a dominant mechanism away from boundaries. We have investigated the influence of stratification at $Re = 1000$, to examine the strong viscous coupling process without introducing the multiple vortex complications associated with higher Reynolds numbers. Figure 6 shows the trajectories for $N = 0.04$, and for $N = 0$ (unstratified) over a total (dimensionless) simulation time of 180 units. The two trajectories are coincident nominally during the initial ground encounter phase. Then, as the relatively higher density fluid is pulled from the ground and around the primary vortex in the stratified case, the body forces produce a more rapid vortex deceleration, as just discussed. Furthermore, the stratification-generated vorticity reduces the vertical vortex rebound and even pushes the primary vortex back toward the symmetry plane. This vertical inhibition and lateral constraint resulting from stratification has also been shown by Delisi et al.,[21] who have observed the more extreme result of complete suppression of vertical rebound motion.

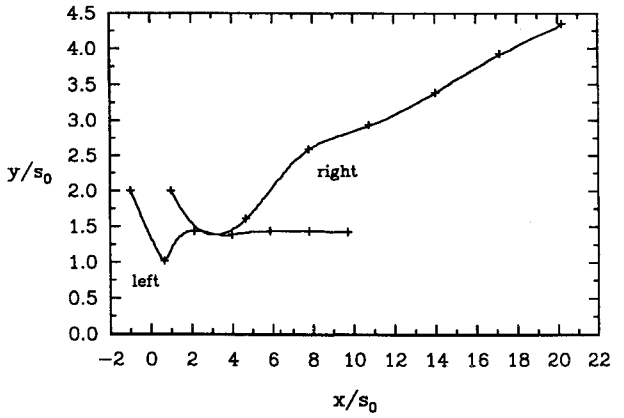

Fig. 8 Influence of crosswind on asymmetric vortex trajectories; Re = 1000, $\delta = s_0$, and $U_\infty = 0.1\Gamma_0/s_0$.

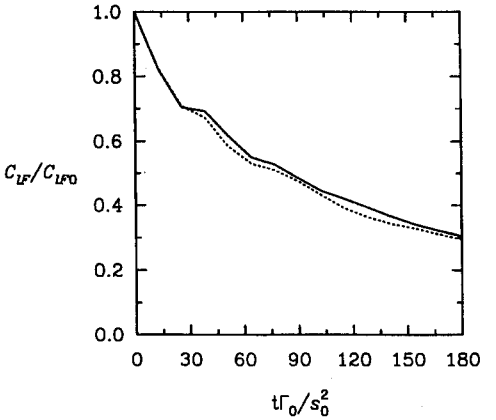

Fig. 9 Influence of nearly constant shear ($\delta = 10s_0, U_\infty = 0.1\Gamma_0/s_0$) on the decay rate of the maximum rolling moment associated with the upwind (left) and downwind (right) vortices; Re = 1000: · · · ·, right and ——, left.

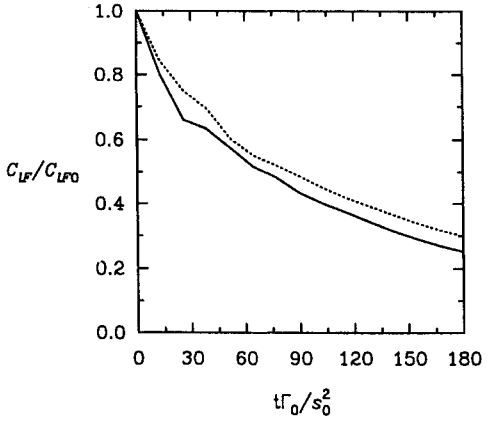

Fig. 10 Influence of a nearly uniform crosswind ($\delta = s_0, U_\infty = 0.1\Gamma_0/s_0$) on the decay rate of the upwind (left) and downwind (right) vortices; (Re = 1000): · · · ·, right and ——, left.

Crosswinds

Surface winds are three dimensional, unsteady, and turbulent. Obviously, a two-dimensional model cannot include head wind effects. Furthermore, we have noted already that the crosswind component eliminates the symmetry boundary conditions (doubling the number of grid points). The portion of the atmospheric boundary layer that exists within an aircraft wing-span height from the ground ($y \leq 2s_0$) coincides nominally with the surface layer (see Stull[38]), which is characterized by nearly constant turbulent transport processes. Between topographic, diurnal, and synoptic effects, virtually any kind of mean crosswind velocity profile shape can exist in that zone as a steady-state condition during the life of an aircraft wake vortex event. (It is assumed that the time scale characterizing mean wind variation is much longer than the corresponding wake vortex decay

time.) Also, since the mechanical energy content of the crosswind is essentially infinite, in comparison to the wake vortex system, a parallel-flow, crosswind profile given by

$$u(\pm\infty, y, t) = U(y) \tag{23}$$

can be assumed. This profile corresponds to an initial vorticity distribution, given by

$$\zeta(x, y, 0) = -\frac{dU}{dy} \tag{24}$$

which is imposed when starting the numerical simulations.

Using a uniform shear layer (flowing from left to right) as a simplified hypothetical crosswind example, we can see from Eq. (24) that the vorticity levels within the computational domain are reduced by a constant amount, during the initialization process. Furthermore, as the simulation is marched forward in time, the negative vorticity introduced upstream by the steady crosswind continues as a source of uniform (negative) vorticity. From a simple interpretation we see that the negative vorticity levels in the upwind primary vortex will become more negative, whereas the downwind primary vortex will exhibit reduced positive vorticity levels eliminating symmetry. On the other hand, since the vorticity produced by viscous coupling with the ground is of opposite sign with its adjacent primary vortex, the upwind vortex is associated with a smaller positive vorticity

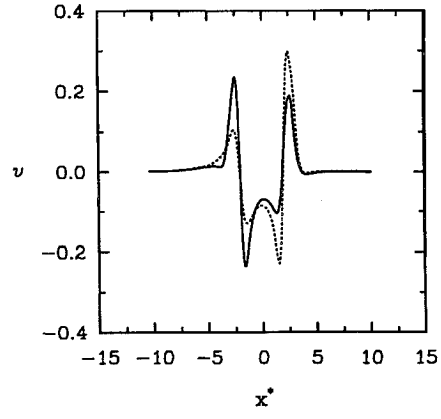

Fig. 11 Vertical velocity distributions in the vicinity of the upwind and downwind vortex cores for a crosswind boundary-layer with thickness, $\delta = s_0(U_\infty = 0.1\Gamma_0/s_0)$, at $\Gamma_0 t/s_0^2 = 30$: · · · ·, right and ——, left.

boundary-layer region. Similarly, the weakened downstream vortex is associated with a strengthened ground plane secondary vortex. The resulting vortex pair system will ultimately rebound nonsymmetrically by rotating counter clockwise into the crosswind. Our simulations have validated this interpretation.

A uniform crosswind, where $U(y) = U_\infty = \text{const}$, is a different extreme. Closer examination, however, reveals that the no-slip boundary condition creates an even stronger negative vorticity contribution along the boundary, exaggerating the asymmetry in the separation zones beneath the descending vortices, thus causing the downwind vortex to rebound more energetically than for the constant shear case. Consequently, the vortex pair appears to rotate counterclockwise or into the wind for both types of crosswind profiles. Since flight observations have been reported for which wake vortex pairs were observed to rotate both into and away from the wind during ground encounter, other wind profiles must be considered. From the wide variety of crosswind velocity profile shapes observed during the Idaho Falls experiments,[18] so-called ground jet profiles were observed occasionally. For those cases, very strong crosswind layers existed in a narrow band within the surface layer. These ground jet profiles, though less common, produce vertical vorticity distributions containing both positive and negative zones, and those profiles cause the vortex pair to rotate in the opposite or clockwise direction.[39]

It is instructive to consider more fundamental crosswind velocity profile types represented by either quasiconstant shear or quasiuniform velocity. We have used von Kármán's integral representation for a laminar boundary layer, where

$$U(y) = U_\infty \begin{cases} 2(y/\delta) - 2(y/\delta)^3 + (y/\delta)^4 & \text{for } y \le \delta \\ 1 & \text{for } y \ge \delta \end{cases} \tag{25}$$

to represent relatively thick and thin shear layer cases. Vortex core trajectories are shown for $U_\infty = 0.1\Gamma_0/s_0$, with $\delta = 10s_0$ (quasiconstant shear) and $\delta = s_0$ (quasiuniform velocity), at $Re = 1000$, in Figs. 7 and 8, respectively. We see that the superposition of negative vorticity because of crosswind shear (discussed earlier) is operative for the thick boundary layer (Fig. 7), whereas a more uniform crossflow occurs for the thin boundary-layer case, causing greater rotation of the vortex pair via the exaggerated separation zone differences.

The corresponding maximum rolling moment decay histories are shown in Figs. 9 and 10 for the thick and thin boundary-layer cases, respectively. Interestingly, the downwind vortex exhibits an almost

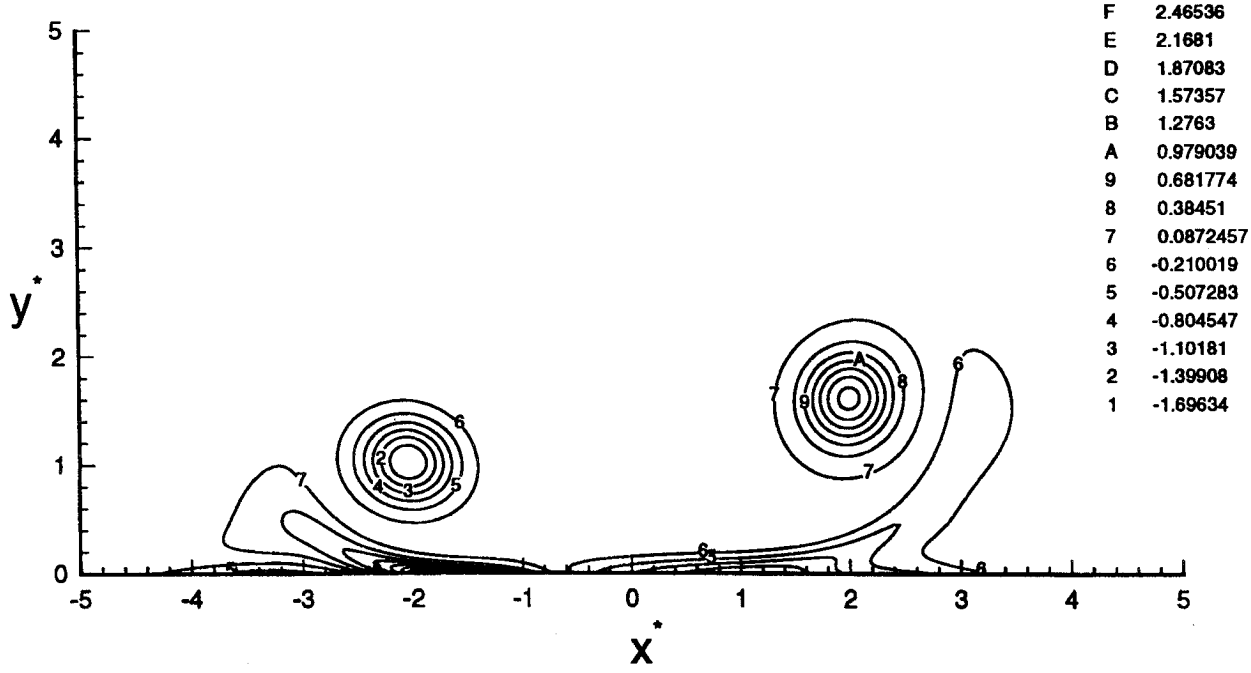

Fig. 12 Vorticity contours at $\Gamma_0 t/s_0^2 = 30$, for the crosswind conditions represented in Fig. 11; $Re = 1000$.

identical decay history for the two cases, whereas the upwind vortex decays much more rapidly in the thin shear layer case where there are obviously larger velocity gradients. The vorticity superposition effect for the thick boundary layer that causes the circulation of the upwind vortex to increase significantly does not appear in the rolling moment history (Fig. 9). The reason for this absence is that the rolling moment depends only on the vertical velocity distribution, although stronger upwind vortex effects are exhibited. In the thin boundary layer case, however, the rolling moment histories (Fig. 10) show that the downwind vortex is stronger. It was noted that the actual flight data, produced in the Idaho Falls tower fly-by tests,[18] indicate that the the upwind vortex circulation levels decay more slowly than the downwind vortex. That difference appears to oppose the relative rolling moment behavior represented in the thin shear layer case. The reason for the higher rolling moment for the downwind vortex can be explained by Fig. 11, which shows the vertical velocity distributions in the vicinity of the upwind and downwind vortex cores (for $\delta = s_0$, $U_\infty = 0.1\Gamma_0/s_0$ at $t = 30$). (The coordinate system is moving in this case, where $x^* = x/s_0 - u_g \cdot \bar{t}$ and the dimensionless grid speed u_g is 0.09.) Further insight can be gained from the corresponding vorticity contour plots ($\bar{t} = 30$), shown in Fig. 12. The upwind vortex is flattened with respect to the boundary, whereas the downwind vortex has its primary elliptic axis oriented in the vertical direction, producing larger vertical velocities. These trends are in agreement with the inviscid predictions of Rossow.[40] From the preceding discussion, it can be seen that the maximum rolling moment coefficient gives better quantification of vortex hazard than the circulation. The roll effects induced from the wake vortex are described more accurately by rolling moment than integration of vorticity within a certain region to calculate circulation. That is because the circulation calculations can include flowfield regions that degrade the implied induced roll hazard estimates for the follower.

IV. Conclusions

A constant eddy viscosity (laminar), two-dimensional vorticity-stream function numerical model has been developed to study the behavior of aircraft wake vortices near the ground. Although the model has limitations, it has yielded new insights concerning the influence of airport weather conditions on wake vortex behavior. We can conclude that increased vortex Reynolds numbers (Γ_0/ν) result in vortex trajectories that approximate closely the inviscid trajectories during closest approach to the ground. Subsequently, the secondary vortices that are generated along the ground produce more robust rebound behavior that is also more complex because of the coupling between the primary and secondary vortices. At lower Reynolds numbers, the secondary vortices dissipate more rapidly and are unable to exert strong influences on the primary vortices. Buoyancy effects have little influence on the initial ground encounter phase of the vortex rebound, because the ground plane inhibits the buoyant torques that result from motion within a stratified fluid away from the ground. On the other hand, stratification always restricts subsequent vortex rebound and lateral propagation.

By neglecting the coupling between follower aircraft and generator aircraft velocity fields, instantaneous rolling moments can be computed for an arbitrarily specified follower wing and can be used to assess wake vortex decay. As long as the specified follower wing is large enough relative to the generator, the excessive core dilation effects are integrated out. These maximum rolling moment histories incorporate the influences of the vortex system (primary and secondary vortices) and airport weather in predicting trends that are related to actual hazard decay. Vortex Reynolds number influences the decay rate more strongly than either stratification or crosswind. Furthermore, the complexity of both the vortex system and the primary vortex trajectories increases with increasing Reynolds numbers. Since the constant eddy viscosity model neglects turbulent details, it may be possible to calibrate the simulations for different aircraft types, where the excessive laminar dilation effects are integrated out by using appropriate follower wing specifications. A nominal equivalent laminar Reynolds number may be developed that reflects the particular generating aircraft size. Further research is needed to address that issue.

Unlike circulation-based decay criteria, the maximum rolling moment considers the local vertical velocity distribution along a specific line segment, and is not subject to the ambiguities associated with circulation domains. Representative maximum rolling moment histories have demonstrated how the secondary vortices produced during ground encounter can alternately enhance then reduce the hazard potential at different times. Simulations have shown that maximum rolling moment histories for the upwind and downwind vortices differ by smaller percentages than do the corresponding circulation histories that are influenced more strongly by the superposition of crosswind vorticity. Depending on the shape of the crosswind velocity profile, the estimated rolling moment hazard can be greater for the downwind vortex than for the upwind vortex, which is counter to the trends indicated by the circulation histories. Furthermore, our simulations have shown that the shape of the crosswind velocity profile can control the rebound behavior of each element of the vortex pair, resulting in unequal rebound amplitudes. Whereas crosswinds normally cause the downwind vortex to rebound higher than the upwind vortex, crosswind profiles that contain so-called ground jets cause the opposite behavior.

Acknowledgments

This research was supported by NASA Langley Research Center, under Grant NAG-1-1437, monitored by Fred H. Proctor. The authors would like to thank George C. Greene for many helpful suggestions and Robert A. Pfouts for his assistance in analyzing the rolling moment data.

References

[1]Machol, R., "Wake Vortices—A Primer," *FAA Aviation Safety Journal*, Vol. 3, No. 1, 1993, pp. 16–19.

[2]Lamb, H., *Hydrodynamics*, Dover, New York, 1932, Sec. 155.

[3]Vicroy, D., Bowles, R., Brandon, J. M., Greene, G. C., Jordan, F. L., Jr., Rivers, R. A., Stewart, E. C., Stough, H. P., III, and Stuever, R. A., "NASA Wake Vortex Research" *19th Congress of the International Council of the Aeronautical Sciences, Proceedings* (Anaheim, CA), Vol. 1, AIAA, Washington, DC, 1994, pp. 519–528.

[4]Donaldson, C. D., and Bilanin, A. J., "Vortex Wakes of Conventional Aircraft," AGARDograph No. 204, May 1975.

[5]Dee, F. W., and Nicholas, O. P., "Flight Measurements of Wing-Tip Vortex Motion near the Ground," Royal Aeronautical Establishment, London, CP-1065, Jan. 1968.

[6]Saffman, P. G., "The Approach of a Vortex Pair to a Plane Surface in Inviscid Fluid," *Journal of Fluid Mechanics*, Vol. 92, 1979, pp. 497–503.

[7]Harvey, J. K., and Perry, F. J., "Flowfield Produced by Trailing Vortices in the Vicinity of the Ground," *AIAA Journal*, Vol. 9, No. 8, 1971, pp. 1659, 1660.

[8]Barker, S. J., and Crow, S. C., "The Motion of Two-Dimensional Vortex Pairs in Ground Effect," *Journal of Fluid Mechanics*, Vol. 82, 1977, pp. 659–671.

[9]Peace, A. J., and Riley, N., "A Viscous Vortex Pair in Ground Effect," *Journal of Fluid Mechanics*, Vol. 129, 1983, pp. 409–426.

[10]Walker, J. D. A., "The Boundary Layer Due to Rectilinear Vortices," *Proceedings of the Royal Society of London*, Series A, Vol. 359, 1978, pp. 167–188.

[11]Ersoy, S., and Walker, J. D. A., "Viscous Flow Induced by a Counter-Rotating Pair of Vortices," *Physics of Fluids*, Vol. 28, No. 9, 1985, pp. 2687–2698.

[12]Doligalski, T. L., Smith, C. R., and Walker, J. D. A., "Vortex Interactions with Walls," *Annual Review of Fluid Mechanics*, Vol. 26, 1994, pp. 573–616.

[13]Orlandi, P., "Vortex Dipole Rebound from a Wall," *Physics of Fluids A*, Vol. 2, No. 8, 1990, pp. 1429–1436.

[14]Bilanin, A. J., Teske, M. E., and Williamson, G. G., "Vortex Interactions and Decay in Aircraft Wakes," *AIAA Journal*, Vol. 15, No. 2, 1977, pp. 250–260.

[15]Bilanin, A. J., Teske, M. E., and Hirsh, J. E., "Neutral Atmospheric Effects on the Dissipation of Aircraft Vortex Wakes," *AIAA Journal*, Vol. 16, No. 9, 1978, pp. 956–961.

[16]Teske, M. E., Bilanin, A. J., and Barry, J. W., "Decay of Aircraft Vortices near the Ground," *AIAA Journal*, Vol. 31, No. 8, 1993, pp. 1531–1533.

[17]Greene, G. C., "An Approximate Model of Vortex Decay in the Atmosphere," *Journal of Aircraft*, Vol. 23, No. 7, 1986, pp. 566–573.

[18]Garodz, L. J., and Clawson, K. L., "Vortex Wake Characteristics of B757-200 and B767-200 Aircraft Using the Tower Fly-by Technique," National Oceanic and Atmospheric Administration, TM ERL-ARL-199, Washington, DC, Jan. 1993.

[19]Drummond, A. M., Onno, R., and Panneton, B., "Trajectories and Stability of Trailing Vortices Very Near the Ground," National Research Council of Canada, Aeronautical Note IAR-AN-74, Ottawa, ON, Canada, Dec. 1991.

[20]Liu, H. T., and Srnsky, R. A., "Laboratory Investigation of Atmospheric Effects on Vortex Wakes," Flow Research, Inc., Rept. No. 497, Belleville, WA, 1990.

[21]Delisi, D. P., Robins, R. E., and Fraser, R. B., "The Effect of Stratification and Wind Shear on the Evolution of Aircraft Wake Vortices Near the Ground: Phase I Results," Northwest Research Associates, Inc., Rept. NWRA-87-R006, Belleville, WA, April 1987.

[22]Robins, R. E., and Delisi, D. P., "Potential Hazard of Aircraft Wake Vortices in Ground Effect with Crosswind," *Journal of Aircraft*, Vol. 30, No. 2, 1993, pp. 201–206.

[23]Zheng, Z. C., and Ash, R. L., "Prediction of Turbulent Wake Vortex Motion near the Ground," *Transitional and Turbulent Compressible Flows*, edited by L. D. Kral and T. A. Zang, ASME Fluids Engineering Div., Vol. 151, American Society of Mechanical Engineers, New York, 1993, pp. 195–207.

[24]Lezius, D. K., "Water Tank Study of the Decay of Trailing Vortices," *AIAA Journal*, Vol. 12, No. 9, 1974, pp. 1065–1071.

[25]Zeman, O., "The Persistence of Trailing Vortices, a Modeling Study," *Physics of Fluids*, Vol. 7, No. 1, 1995, pp. 135–143.

[26]Zheng, Z. C., and Ash, R. L., "Viscous Effects on a Vortex Wake in Ground Effect," *Proceedings of the FAA International Wake Vortex Symposium*, Vol. 2, edited by J. N. Hallock, U.S. Dept. of Transportation, 1991, pp. 31-1–31-30.

[27]Arakawa, A., "Computational Design for Long-Term Numerical Integration of the Equations of Motion: Two-Dimensional Incompressible Flow: Part I," *Journal of Computational Physics*, Vol. 1, No. 1, 1966, pp. 119–143.

[28]Zilliac, G. C., Chow, J. S., Dacles-Mariani, J., and Bradshaw, P., "Turbulent Structure of a Wingtip Vortex in the Near Field," AIAA Paper 93-3011, July 1993.

[29]Batchelor, G. K., "Axial Flow in a Trailing Vortex," *Journal of Fluid Mechanics*, Vol. 20, 1964, pp. 645–658.

[30]Phillips, W. R. C., and Graham, J. A. H., "Reynolds-Stress Measurements in a Turbulent Trailing Vortex," *Journal of Fluid Mechanics*, Vol. 147, 1984, pp. 353–371.

[31]Zheng, Z. C., "The Influence of Reynolds Number and Atmospheric Effects on Aircraft Wake Vortices Near the Ground," Ph.D. Dissertation, Mechanical Engineering and Mechanics Dept., Old Dominion Univ., Norfolk, VA, May 1993.

[32]Landau, L. D., and Lifshitz, E. M., *Fluid Mechanics*, Pergamon, New York, 1966, Sec. 4.

[33]Gresho, P. M., "Incompressible Fluid Dynamics: Some Fundamental Formulation Issues," *Annual Review of Fluid Mechanics*, Vol. 26, 1994, pp. 573–616.

[34]Zheng, Z. C., "A Consistent Boundary Condition for Vorticity/Stream-Function Simulations of Wall-Bounded Vortex Flows," *Proceedings of the 9th International Conference on Numerical Methods in Laminar and Turbulent Flow* (Atlanta, GA), edited by C. Taylor and P. Durbetaki, Vol. 9, Pt. 1, Pineridge, Swansea, Wales, UK, 1995, pp. 179–190.

[35]Swartztrauber, P. N., and Sweet, R., "Algorithm 541, Efficient FORTRAN Subprogram for the Solution of Separable Elliptic Partial Differential Equations [D3]," *ACM Transactions on Mathematical Software*, Vol. 5, 1979, pp. 352–364.

[36]Ferziger, J. H., "Estimation and Reduction of Numerical Error," *Quantification of Uncertainty in Computational Fluid Dynamics*, edited by I. Celik, C. J. Chen, P. J. Roache, and G. Scheuerer, ASME Fluids Engineering Division, Vol. 158, American Society of Mechanical Engineers, New York, 1993, pp. 1–7.

[37]Ash, R. L., Zheng, Z. C., and Greene, G. C., "Cross Wind Effects on Turbulent Aircraft Wake Vortices Near the Ground," AIAA Paper 94-2381, June 1994.

[38]Stull, R. B., *An Introduction to Boundary Layer Meteorology*, Kluwer Academic, Dordrecht, The Netherlands, 1988.

[39]Zheng, Z. C., Ash, R. L., and Greene, G. C., "A Study of the Influence of Cross Flow on the Behavior of Aircraft Wake Vortices near the Ground," *19th Congress of the International Council of the Aeronautical Sciences, Proceedings* (Anaheim, CA), Vol. 2, AIAA, Washington, DC, 1994, pp. 1649–1659.

[40]Rossow, V. J., "Convective Merging of Vortex Cores in Lift-Generated Wakes," AIAA Paper 76-415, July 1976.